International Journal of the Physical Sciences Vol. 6(4), pp. 917-929, 18 February, 2011
Available online at http://www.academicjournals.org/IJPS
DOI: 10.5897/IJPS10.510
ISSN 1992 - 1950 ©2011 Academic Journals

Full Length Research Paper

Using spectral mapping techniques on short wave infrared bands of ASTER remote sensing data for alteration mineral mapping in SE Iran

Amin Beiranvnd Pour, Mazlan Hashim* and Maged Marghany

Institute of Geospatial Science and Technology (INSTeG) Universiti Teknologi Malaysia, 81310 UTM Skudai, Johor Bahru, Malaysia.

Accepted 27 January, 2011

Spectral mapping techniques were applied on shortwave infrared of advanced spaceborne thermal emission and reflection radiometer (ASTER) data for discriminating between hydrothermal alteration zones, and the identification of high potential mineralized lithologic unit associated with hydrothermal porphyry copper mineralization in the Central Iranian Volcanic Belt. In this study, shortwave infrared radiations of ASTER data were processed with spectral angle mapping, linear spectral unmixing, matched filtering, and mixture tuned matched filtering techniques. Two copper mining districts were used as reference to demonstrate the applicability of the spectral mapping techniques for spectral distinction of specific hydrothermal alteration zones such as argillic, phyllic and propylitic. The results of this study showed that spectral information can be used for generating spatial alteration mineral maps for purely virgin regions, and it can provide a cost-effective method to discriminate the new prospects for porphyry copper exploration prior to detailed and costly ground investigations.

Key words: ASTER, spectral mapping techniques, hydrothermal alteration minerals, copper exploration.

INTRODUCTION

The advanced space-borne thermal emission and reflection radiometer (ASTER) is a remote sensing sensor with enhanced capabilities for mineral exploration, which was built by Japan's Ministry of Economy Trade and Industry (METI), and launched by NASA on EOS/Terra platform on 18th December 1999. ASTER is a multispectral sensor with 14 bands that can measure reflected and emitted electromagnetic radiation from Earth's surface in three subsystems consisting of (i) visible and near infrared radiation (VNIR); (ii) shortwave infrared radiation (SWIR); (iii) thermal infrared radiation (TIR).

The spatial resolution of three recording bands in (VNIR) between 0.52 and 0.86 µm and six bands in (SWIR) from 1.6 to 2.43 µm and five bands in (TIR) the 8.125 to11.65 µm wavelength region are 15 and 30 and 90 m, respectively (Yamaguchi et al., 1999; Abrams, 2000). The technical characteristics of ASTER data are shown in the Table 1. The six spectral bands of the ASTER SWIR subsystem were designed to measure reflected solar radiation in order to distinguish Al-OH, Fe, Mg-OH, Si-O-H, and CO3 absorption features (Abram and Hook, 1995). Previous studies documented identification of specific hydrothermal alteration minerals, such as alunite, kaolinite, calcite, dolomite, chlorite, talc and muscovite, as well as mineral groups, through analysis of ASTER SWIR data, which have been proven using in-situ field spectral measurements (Rowan et al., 2006; Ducart et al., 2006; Di Tommaso and Rubinstein, 2007). Therefore, these properties making SWIR of ASTER data suitable for detailed mineralogical alteration mapping, that is important to distinguish the high

*Corresponding author. E-mail: mazlanhashim@utm.my, profmhashim@gmail.com. Tel: +607- 5530666. Fax: +607-5531174.

Table 1. ASTER instrument characteristics (Yamaguchi et al., 1999).

Characteristic	VNIR	SWIR	TIR
Spectral range (μm)	Band 1: 0.52–0.60, Nadir looking Band 2: 0.63–0.69, Nadir looking Band 3: 0.76–0.86, Nadir looking Band 3: 0.76–0.86, Backward looking	Band 4: 1.600– 1.70 Band 5: 2.145– 2.185 Band 6: 2.185– 2.225 Band 7: 2.235– 2.285 Band 8: 2.295– 2.365 Band 9: 0.360– 2.430	Band 10: 8.125–8.475 Band 11: 8.475–8.825 Band 12: 8.925–9.275 Band 13: 10.25–10.95 Band 14: 10.95–11.65
Ground resolution (m)	15	30	90
Swath width (km)	60	60	60
Singnal quantization level (bits)	8	8	12

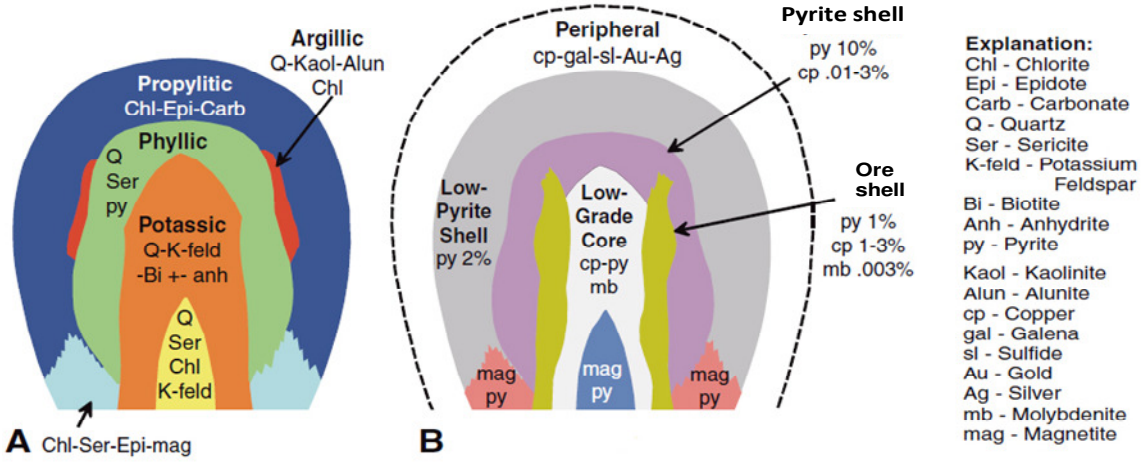

Figure 1. Hydrothermal alteration zones associated with porphyry copper deposit (Modified from Lowell and Guilbert, 1970; Mars and Rowan, 2006). (A) Schematic cross section of hydrothermal alteration mineral zones, which consist of propylitic, phyllic, argillic, and potassic alteration zones. (B) Schematic cross section of ores associated with each alteration zone.

potential areas of economical mineralization of ore deposits such as epithermal gold and hydrothermal porphyry copper deposits. Each ideal porphyry copper deposit is typically characterized by hydrothermal alteration mineral zones (Figure. 1) (Lowell and Guilbert, 1970). A core of quartz and potassium-bearing minerals is surrounded by broad phyllic zone and narrower argillic and the outer propylitic zones. These multiple zones are containing minerals with diagnostic spectral absorption features in SWIR portion of the electromagnetic spectrum, which can be distinguishable from each other by SWIR of ASTER data (Hunt and Ashley, 1979; Mars and Rowan, 2006). The broad phyllic zone is characterized by illite/muscovite (sericite) that indicate an intense Al-OH absorption feature centered at 2.20 μm coincide with ASTER band 6, and the narrower argillic zone including, kaolinite and alunite that display a secondary Al-OH absorption feature at 2.17 μm correspond with ASTER band 5. The mineral assemblage of the outer propylitic zone are epidote, chlorite, and calcite that exhibit absorption features situated in the 2.35 μm that coincide with ASTER band 8 (Figure 2) (Hunt and Ashley, 1979; Mars and Rowan, 2006). The differentiation between alteration zones and the identification of phyllic zone are important in the exploration of porphyry copper mineralization, because phyllic zone can be an indicator of high potential area with economical mineralization of copper ore shell (Figure 1) (Lowell and Guilbert, 1970).

In this paper, spectral mapping techniques such as spectral angle mapping (SAM), linear spectral unmixing (LSU), matched filtering (MF), and mixture tuned

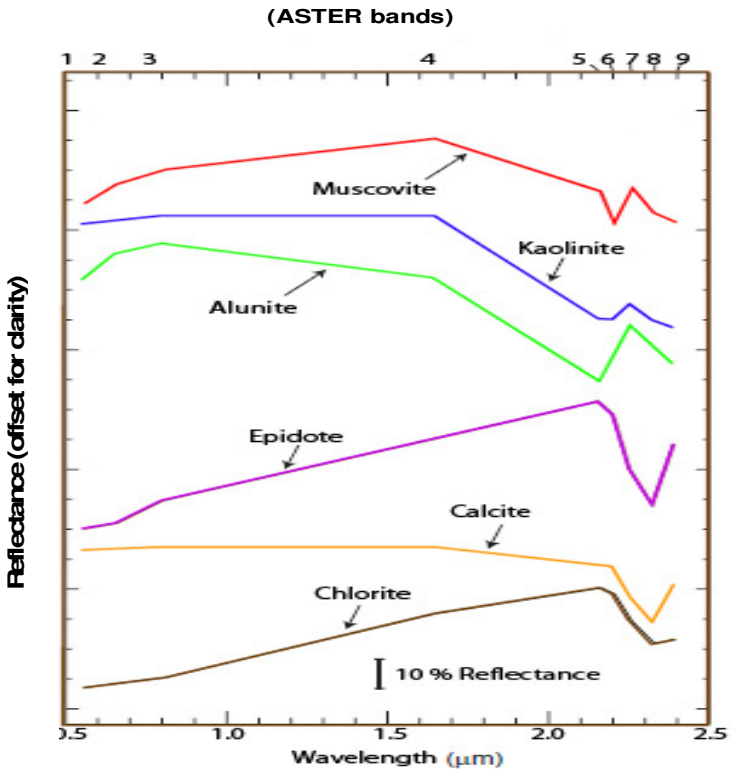

Figure 2. Laboratory spectra of muscovite, kaolinite, alunite, epidote, calcite, and chlorite resampled to ASTER bandpasses. Spectra include muscovite, typical in phyllic alteration zone, with a 2.20 µm absorption feature; kaolinite and alunite, which are common in argillic alteration zone, have 2.17 µm absorption features; and epidote, calcite, and chlorite, which are typically associated with propylitic alteration zone and display 2.35 µm absorption features (Clark et al., 1993b; Mars and Rowan, 2006).

matched filtering (MTMF) were applied on SWIR of ASTER data to discriminate the specific hydrothermal alteration zones associated with porphyry copper mineralization in two well-known mining districts in SE Iran. The results can be as a guide in delimiting the high potential mineralized lithologic units with respect to the surrounding country rocks.

GEOLOGICAL SETTING

The major part of Iran is semi-arid with well-exposed and spars vegetated surface, which is ideal for remote sensing geological mapping. The Central Iranian Volcanic Belt with trending NW-SE, located on the Tethyan Copper Belt in Iran. It is classified as an Andean Volcanic arc (Alavi, 1980; Berberian et al., 1982). In Iran, all known porphyry copper mineralization are concentrated in this belt (Figure 3). It is the product of Tethys oceanic plate subduction under the Iranian micro-plate followed by continent-to-continent collision of the Arabian and Eurasian plates (Regard et al., 2004). Porphyry copper deposits in this belt are associated with Miocene adakite-like orogenic granitoids which intruded the Eocene volcanic rocks (Shafiei et al., 2009). The Central Iranian Volcanic Belt is a volcano-plutonic complex contains extrusive and intrusive rocks of Eocene to Quaternary age (Stocklin, 1974; Farhoudi, 1978). Geochemical investigations have shown that this volcanic belt generally consists of subduction-related calc-alkaline rocks (Forster et al., 1972; Berberian et al., 1982; Shahabpour, 2005, 2007).

In this belt, mountains include a volcanic succession of Eocene calc-alkaline basaltic andesites and Oligocene shoshonitic rocks intruded by Neogene quartz diorites, quartz monzonites, and granodiorites which contain vein type and porphyry copper mineralization. Additional plutonic rocks include granite and gabbro, and volcanic rocks contain basalt, andesite, and dacite, which were erupted as lava flows, ignimbrites, and pyroclastic flows (Huber, 1969; Hassanzadeh, 1993). The most of volcanism occurred from Eocene to Miocene time in this belt (Huber, 1969; Dimitrijevic, 1973; Hajian, 1977; Amidi, 1984). Extensive mineralization occurred from Miocene to

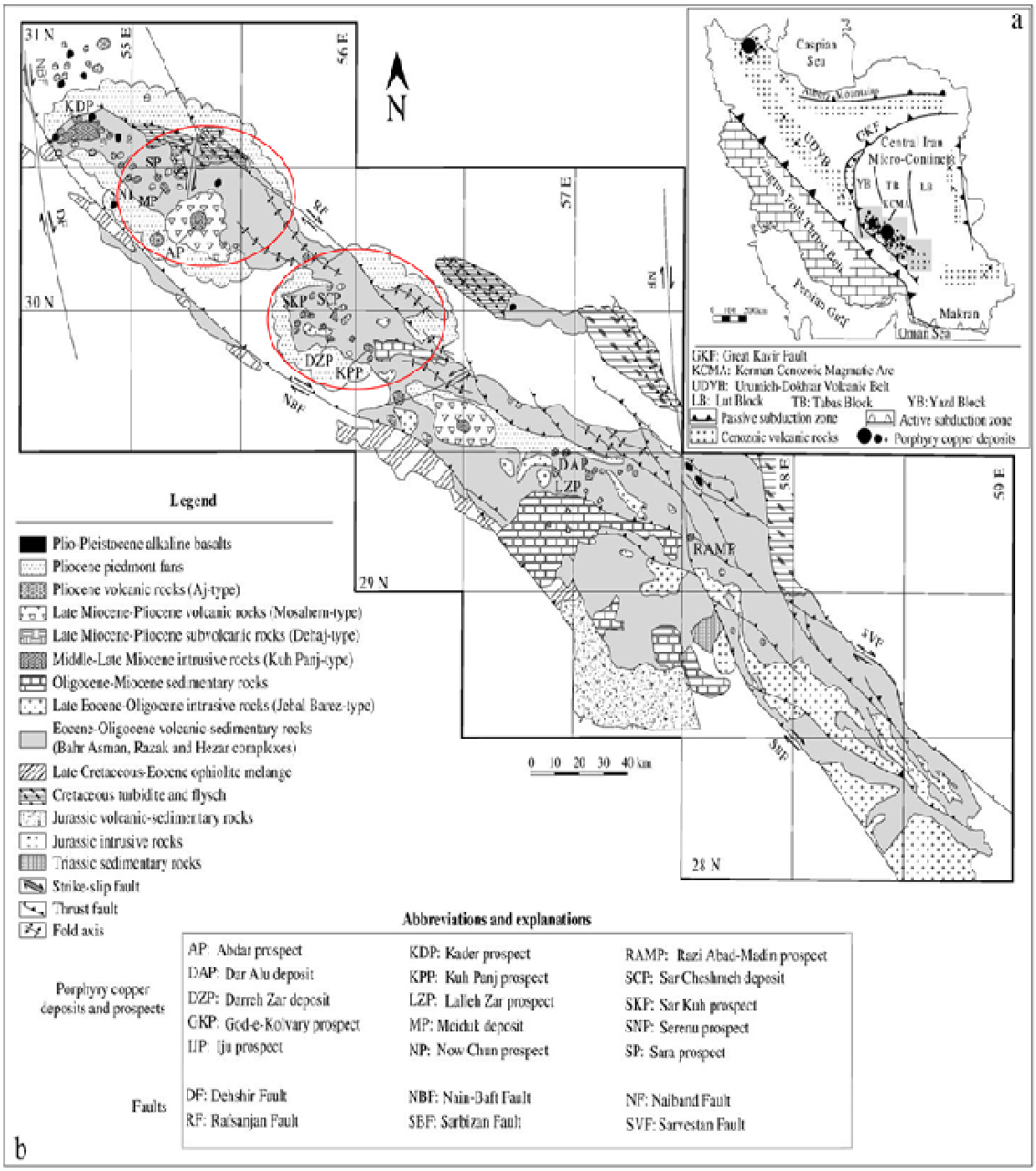

Figure 3. (a) Location of the Central Iranian volcanic belt and distribution of porphyry Cu deposits in Iran. (b) Simplified litho-structural map of the southeastern of the volcanic belt and location of major porphyry Cu deposits and prospects (Shafiei, 2010). Study areas are located in ellipsoidal polygons.

Pliocene time and produced porphyry copper and vein-type mineralization. Giant porphyry copper ore deposits in this belt, including Sarcheshmeh and Meiduk are in a granodiorite and a quartz diorite, respectively (Hassanzadeh, 1993).

In this volcanic belt the abundance of known porphyry copper deposits reflects the economic potential importance, and also warranting the exploration of new

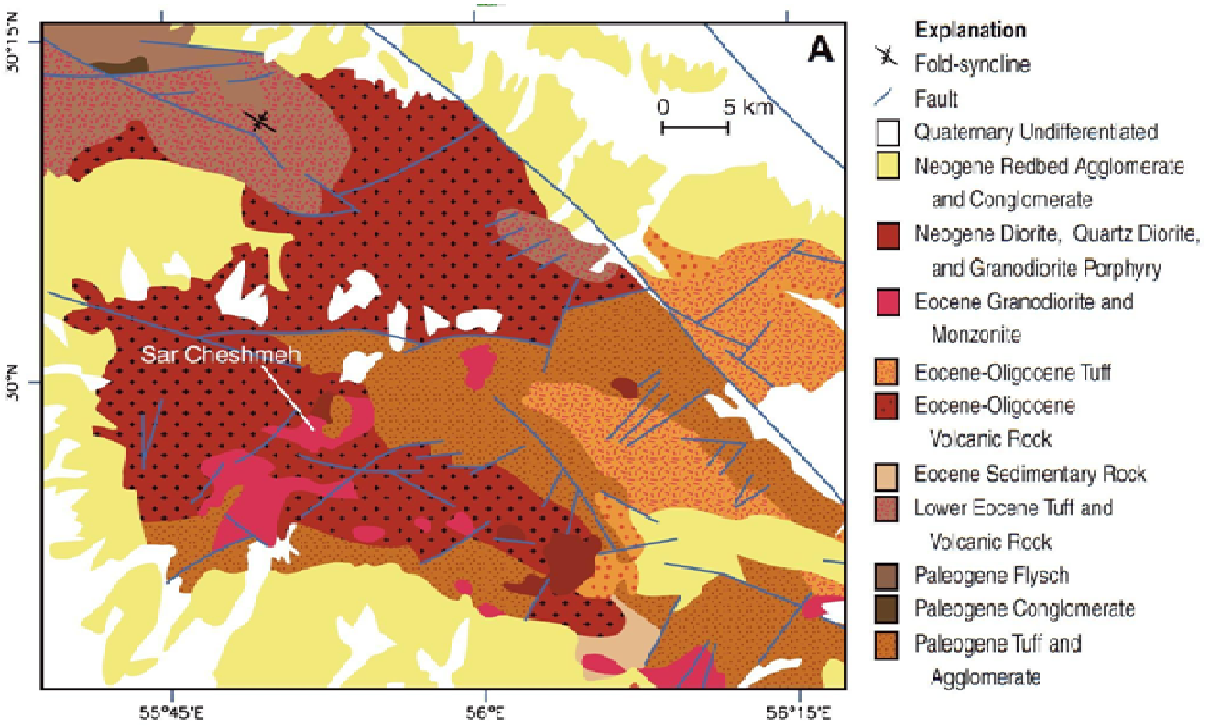

Figure 4. Geological map of Sarcheshmeh region (Modified from Huber, 1969).

prospects. Therefore, it is the best candidate with great potential for exploration new prospects of porphyry copper and vein-type epithermal gold deposits by ASTER remote sensing data.

This study focuses on two giant and largest deposits: (i) Sarcheshmeh; and (ii) Meiduk porphyry copper deposits, where Cu and Mo are currently mined. The Sarcheshmeh porphyry copper deposit (55° 52′ 20″ E, 29° 58′ 40″ N) is located 60 Km southwest of Kerman city. The deposit is within a belt of Eocene volcanic rocks and Oligo-Miocene subvolcanic granitoid rocks. The oldest host rocks at the Sarcheshmeh porphyry copper deposit belong to an Eocene volcanogenic complex, also known as the Sarcheshmeh complex (Waterman and Hamilton, 1975). The complex consists of pyroxene trachybasalt, pyroxene trachyandesite of potassic and shoshonitic affinity (Aftabi and Atapour, 1997), less abundant andesite and rare occurrences of agglomerate, tuff, and tuffaceous sandstone (Figure 4). These were intruded by a complex series of Oligo-Miocene granitoid intrusive phases such as quartz diorite, quartz monzonite and granodiorite. The granitoid rocks are cut by a series of intramineral hornblende porphyry, feldspar porphyry and biotite porphyry dykes (Waterman and Hamilton, 1975). Hydrothermal alteration and mineralization at Sarcheshmeh are centered on the stock and were broadly synchronous with its emplacement. Early hydrothermal alteration was dominantly potassic and propylitic, and was followed later by phyllic, silicic, and argillic alteration (Hezarkhani, 2006).

On the other hand, the Meiduk porphyry copper deposit (55° 10′ 05″ E, 30° 25′ 10″ N) is located 45 km northeast of Shahr-e-Babak, Kerman province. Figure 5 shows geological map of the Meiduk area. Lower Eocene rocks are parts of a volcanic complex consisting of rhyolite lavas, breccias, acidic tuffs, and pyroclastic rocks. This volcanic complex followed by another Eocene to Oligocene volcanic complex, which consists of trachybasalt, andesite and trachyandesite, andesite-basalt, and acidic tuff. The intrusive rocks were emplaced into the volcanic rocks as stock dykes at the Meiduk ore deposit. The volcanic complexes and intrusive rocks are partly covered by late Miocene-Pliocene volcanic and subvolcanic rocks of the Masahim stratovolcano (Hassanzadeh, 1993). The youngest volcanic rocks in the study area are quaternary in age and range from trachyte to dacite. The Cu-mineralization and associated hydrothermal alteration zones are focused on the Miocene dioritic Meiduk porphyry and Eocene andesitic rocks (Boomeri et al., 2009). However, distribution of the various alteration types is irregular. The concentric alteration zones from the centre outward are potassic, phyllic, and propylitic. This pattern is similar to alteration envelopes that are associated with many other porphyry Cu–Mo deposits. Amiraie, (1991) recognized potassic, phyllic, argillic, and propylitic alteration zones at Meiduk

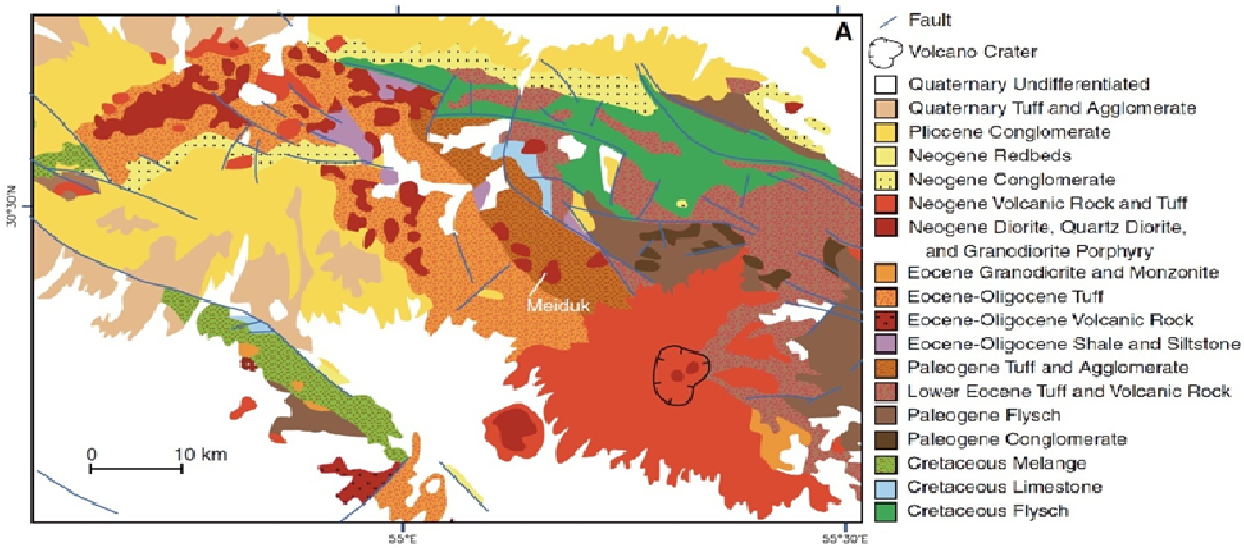

Figure 5. Geological map of Meiduk region (Modified from Huber, 1969).

area.

DATA CALIBRATION AND IMAGE PROCESSING METHODS

Two cloud-free level 1B ASTER scenes used in this study were acquired over Sarcheshmeh and Meiduk areas on June 20th, 2006 and July 15th, 2007, respectively. The level 1B data product measures radiance at the sensor, without atmospheric corrections and were produced from the original level 1A format by Earth and Remote Sensing Data Analysis Center (ERSDAC) Japan. The 1B format data also has been applied for both geometric and radiometric corrections (Abrams, 2000). The images have been pre-georeferenced to UTM zone 40 North projection with WGS-84 datum. The calibration and data analysis steps implemented to the original ASTER scenes are as follows.

The crosstalk correction was performed to data set, aimed at removing the effects of energy overspill from band 4 into bands 5 and 9 (Iwasaki and Tonooka, 2005). In doing so, the Cross-Talk correction software that is available from www.gds.aster.ersdac.or.jp was used. Atmospheric correction was applied by fast line-of-sight atmospheric analysis of spectral hypercubes (FLAASH) algorithm on SWIR subsystem (Thome et al., 1998). In addition, the ASTER Level 1B data converted to reflectance using the Internal average relative reflection (IARR) method. Ben-Dor et al. (1994) recommended IARR reflectance technique for mineralogical mapping as the preferred calibration technique which does not require a prior knowledge of samples collected from the field area. ASTER SWIR surface reflectance scene of the study area were processed and analyzed by environment for visualizing images (ENVI) 4.5 software package.

With spectral mapping techniques such as spectral angle mapping, linear spectral unmixing, matched filtering and mixture tuned matched filtering, pixels that have mixed spectral signatures are extractable and can be separated from the undesirable background, and thus mineral abundance maps can produce free of diluting effects of the environment. Performing these techniques for mapping surface mineralogy are often based on the comparison of image reflectance spectra with library spectra of end-member minerals, which are presented at the ground surface.

In this investigation, the spectra of selected end-member minerals have been taken from the ASTER spectral library version 2.0; which can be ordered from http://speclib.jpl.nasa.gov/ (Baldridge et al., 2009). We selected the spectra of dominated end-member minerals consist of muscovite (K Al2(Si Al3) O10(OH,F)2 as the indicator of phyllic zone, and kaolinite (Al2 Si2 O5 (OH) 4) as the indicator of argillic zone, and epidote (Ca2(Al Fe3+)3O (SiO4)(SiO7)(OH) as the indicator of propylitic zone to discriminate the alteration zones, respectively. Figure 2 shows the spectral characteristics of the three minerals of interest that re-sampled to ASTER bandpasses. The spectral absorption feature of muscovite as indicator of phyllic zone is centered at 2.20 µm coincide with ASTER band 6, kaolinite as indicator of argillic zone at 2.17 µm correspond with ASTER band 5 and epidote as indicator of propylitic zone at 2.35 µm coincide with ASTER band 8 (Figure 2) (Mars and Rowan 2006).

RESULTS AND DISCUSSION

Alteration mapping

We applied spectral mapping techniques on SWIR subsystem of ASTER data to map the surface mineralogy of hydrothermal alteration zones related to porphyry copper mineralization in Sarcheshmeh and Meiduk regions.

The spectral angle mapping (SAM) is a classification technique that permits rapid mapping by calculating the spectral similarity between the image spectrums to reference reflectance spectra. SAM measures the spectral similarity by calculating the angle between the two spectra, treating them as vectors in n-dimensional space (Kruse et al., 1993). This technique applied on two full ASTER scenes of Mieduk and Sarcheshmeh regions.

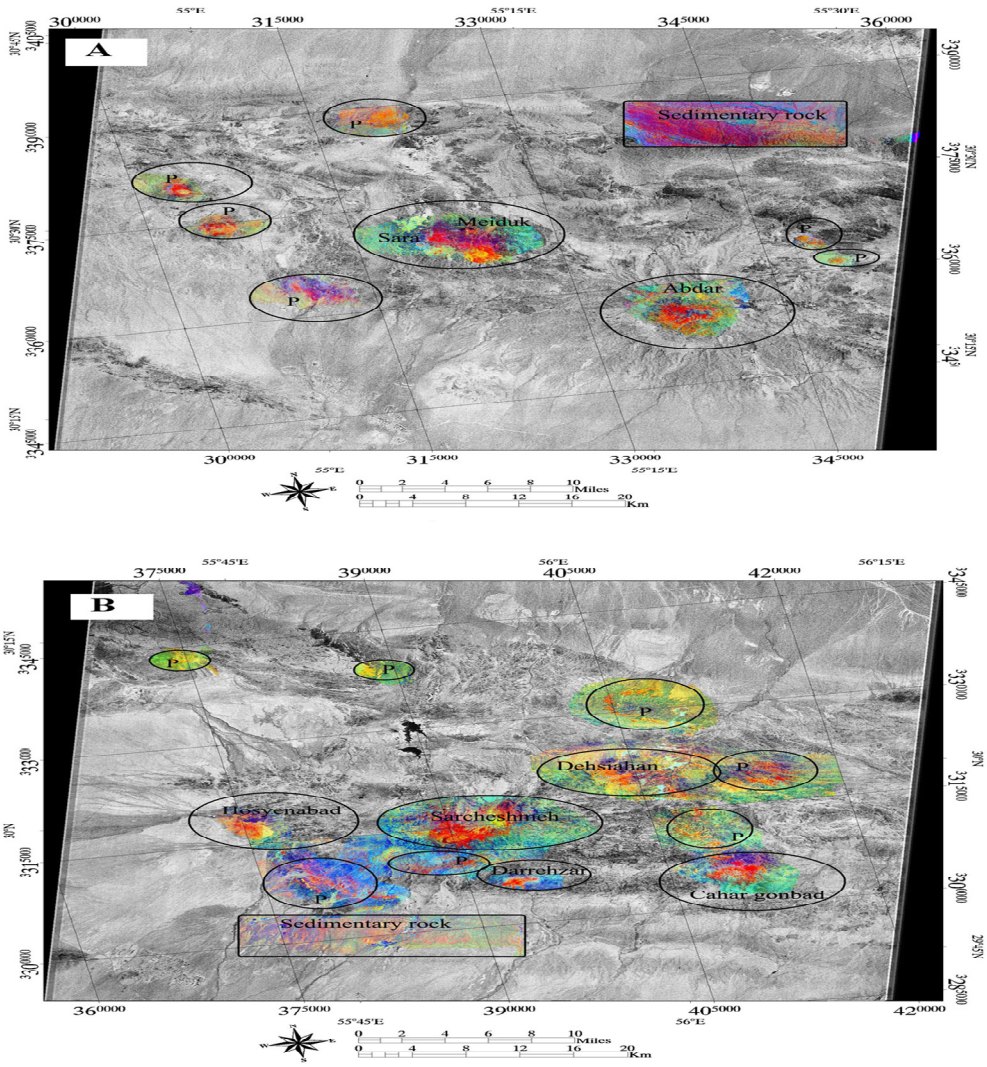

Figure 6. False colour composites of muscovite, kaolinite, and epidote SAM rule image. Alteration halos are depicted ellipsoidal polygons, known copper deposits highlighted by their names. New identified alteration halos are marked by (P). Sedimentary rocks are located inside rectangles, in the (A) Meiduk; and (B) Sarcheshmeh region.

SAM technique was implemented according to optimal threshold angles (radians), so as to avoid spectral confusion with other minerals and minimize the number of unclassified pixels. The optimal threshold angles (radians) for indicator minerals are 0.01 for muscovite, 0.05 for kaolinite and 0.03 for apidote (Castro, 2004). The output from SAM is a set of grey-scale rule images (one per mineral end-member). We assigned false colour composite to muscovite, kaolinite and epidote rule images, respectively. Results exhibited the differences between hydrothermal alteration zones (Figure 6 A-B). The broad red areas are phyllic zone, the locally narrower green areas are argillic zone, and blue areas are propylitic zone that surround phyllic and argillic zones.

According to previous remote sensing and geology studies in this area (Tangestani and Moore, 2002; Ranjbar et al., 2004; Mars and Rowan, 2006; Tangestani, et al., 2008), this technique efficiently revealed the alteration halos around known copper deposits and also new prospects have been identified, which is marked by (P) in Figure 6 (A-B). Unfortunately, in comparison with geologic maps there is some interference of sedimentary rocks (inside rectangles) as red to light red colour in north of Meiduk scene and south of Sarcheshmeh scene. Sedimentary rocks (mudstone, shale, claystone, etc.) can play a role such an erroneous material in mapping hydrothermal alteration minerals because of large amounts of detrital clays such as montmorillonite, illite,

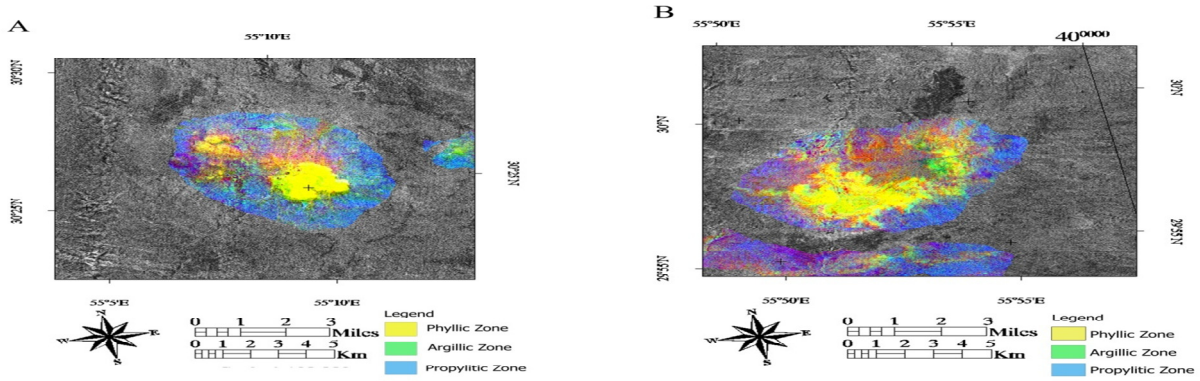

Figure 7. (A) Abundance image from unmixing end members on subscene of Meiduk and Sara mines. (B) Sarcheshmeh mine.

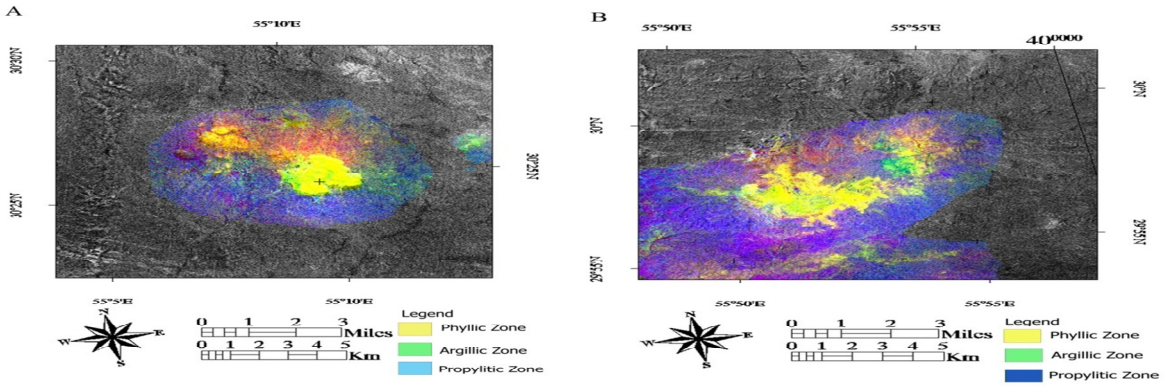

Figure 8. (A) MF score image of end members on subscene of Meiduk and Sara mines. (B) Sarcheshmeh mine.

muscovite and kaolinite in their compositions (Mars and Rowan, 2006).

Because of the presence of sedimentary rocks in study area and by the virtue of their role as erroneous materials in the mapping alteration zones and the difficulty of recognition of specific alteration zones in regional scale. Hereafter, we have selected two subscene windows (500x500 pixels) extracted from ASTER full scenes consist of Mieduk, Sara and Sarcheshmeh mines. We used them as test sites for applying linear spectral unmixing (LSU), matched filtering and mixture tuned matched filtering techniques.

Linear spectral unmixing (LSU) technique is used to determine the relative abundance of materials that are depicted in multispectral or hyperspectral imagery based on the materials' spectral characteristics. The reflectance at each pixel of the image is assumed to be a linear combination of the reflectance of each material (or end-member) present within the pixel. This technique also known as sub-pixel sampling, or spectral mixture analysis, is a widely used procedure to determine the proportion of constituent materials within a pixel based on the materials' spectral characteristics (Boardman, 1992). The unconstrained unmixing algorithm was performed on selected subscenes. The visual results displayed a series of gray scale images, one for each end-member; false colour composite assigned to muscovite, kaolinite and epidote abundance images, respectively.

The achieved results manifested phyllic zone as yellow, argillic zone as green and propylitic zone as blue colour that surround phyllic and argillic zones (Figure 7 A-B).

The matched filtering (MF) technique performs a partial unmixing of spectra to estimate the abundance of user-defined end members from a set of reference spectra. This technique maximizes the response of the known end member and suppresses the response of the composite unknown background, thus matching the known signature (Boardman et al., 1995). Figure 8 (A-B) is shown the MF score images for each selected end-members as false colour composite assigned to MF score images for

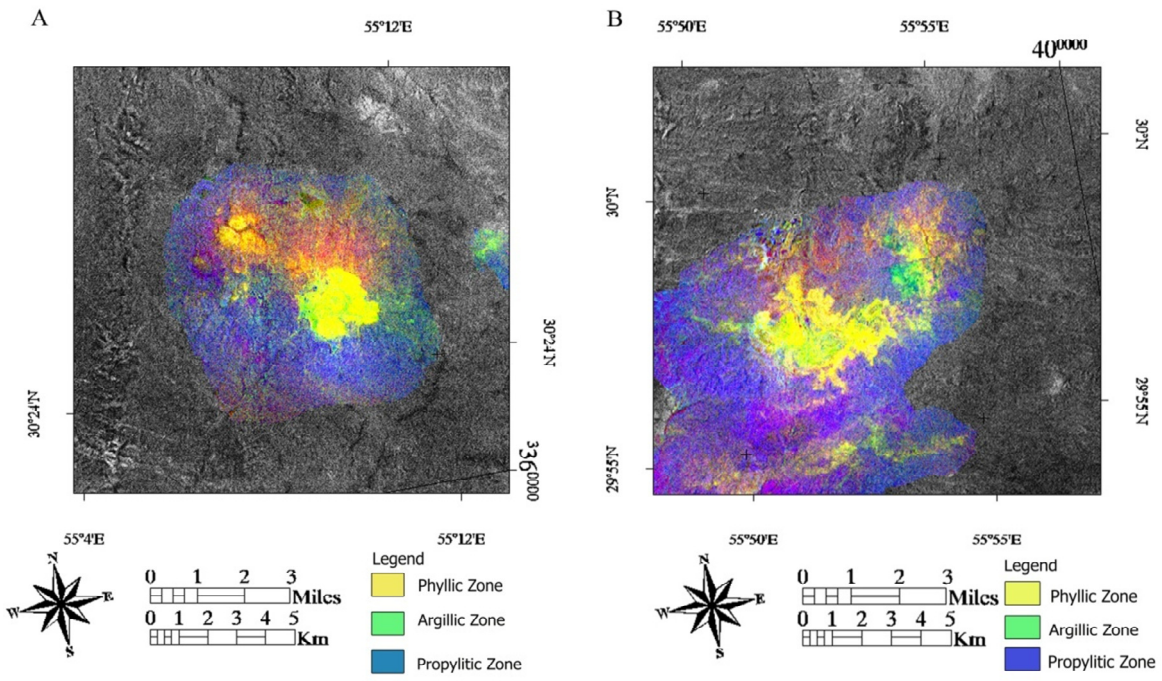

Figure 9. (A) MF score image derived of MTMF results for each end member on subscene of Meiduk and Sara mines. (B) Sarcheshmeh mine.

making easier to distinguish alteration zones. The derived results revealed phyllic zone as yellow colour, argillic zone as green and propylitic zone as blue colour.

Mixture tuned matched filtering (MTMF) technique is a combination of the best parts of the linear spectral mixing model and the statistical matched filter model while avoiding the drawbacks of each parent method (Boardman, 1998). The derived results of this technique were presented as grey scale images; false colour composite generated to show the distribution of indicator minerals (end-members) in order to the differentiation of alteration zones (Figure 9 A-B). Results showed phyllic zone as yellow colour, argillic zone as green and propylitic zone blue colour.

FIELD VERIFICATION

The identified alteration zones from processed ASTER images are verified with in-situ inspection. The field photographs of the geomorphology, rock units and porphyry copper deposits in the study area are shown in Figure 10 (A-F). Moreover, systematic rocks sampling of identified alteration zones were carried out to measure spectral reflectance and mineralogical descriptions. X-Ray diffraction (XRD) was applied for analyzing bulk mineralogy and spectral reflectance analysis using analytical spectral devices (ASD). X-ray diffraction (XRD) analysis was implemented by D8ADVANCE X-ray diffractometer on rock samples. The minerals predominantly detected in the specific alteration zones including muscovite, illite and quartz in phyllic zone, kaolinite and quartz in argillic zone, and epidote, chlorite, calcite and quartz in propylitic zone, respectively (Figure 11 A-C). Spectral reflectance measurements were made using an analytical spectral devices (ASD) filed-portable spectrometer Fieldspac® HandHeld (HH) model, which records a reflectance spectrum across an overall spectral range of 325 to 2500 nanometer (nm) with a 10 nm individual band width. Figure 12 (A-C) indicates spectra of rocks samples for specific alteration zones. It should be noted that all results were observed in a laboratory condition. Spectral reflectance was measured using an artificial light source. The spectra of phyllic rock sample exhibited absorption features in 2200 nm, as shown in Figure 12 A, Argillic rock sample in 2170 nm and 2200 nm and propylitic rock sample in 2350 nm, which are shown in Figure 12 B and C. Figure 13 shows the alteration maps of Sarcheshmeh mine (Waterman and Hamilton, 1975; Jacobsen, 1975), which used to verify the results of the present investigation. In compare with this map, delimited alteration zones in the processed images were situated in correct locations. Thus, phyllic and propylitic zones were identified quite well in the processed images, and Argillic zone was also discriminated as small parts of alteration system.

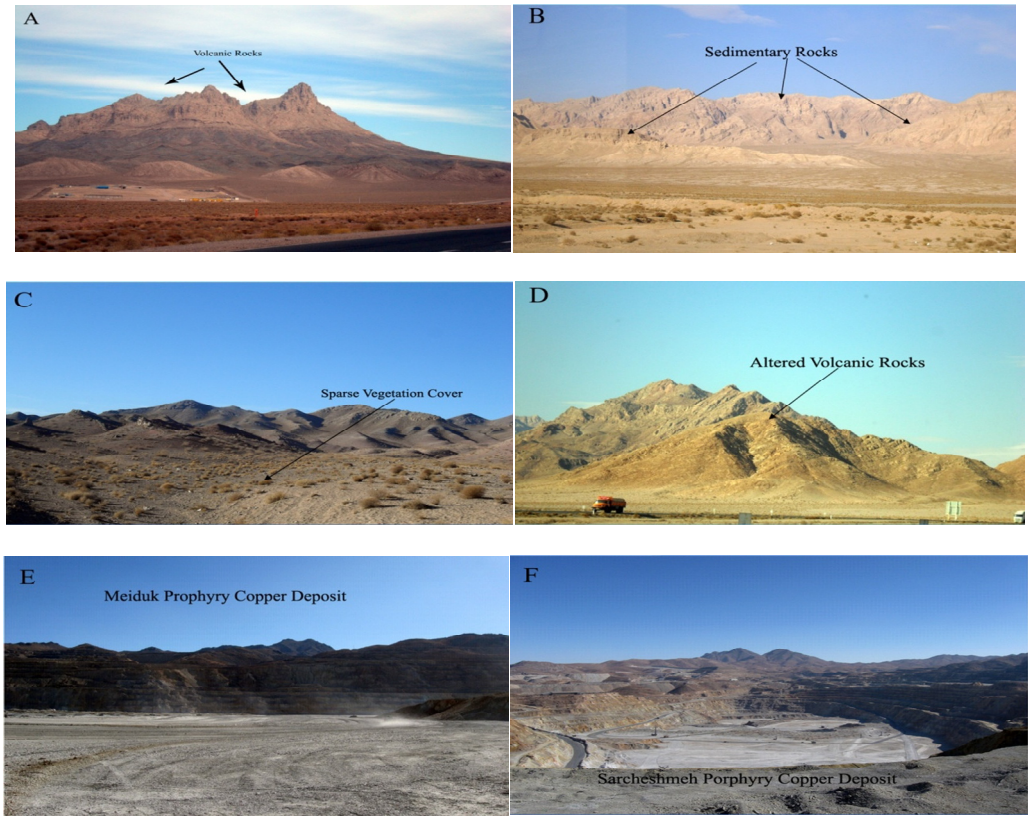

Figure 10. Field photograph of the geological structures of the study area (A) Regional view of volcanic rocks; (B) Sedimentary rocks; (C) View of the distribution of vegetation; (D) Altered volcanic rocks; (E) Meiduk porphyry copper deposit; (F) Sarcheshmeh porphyry copper deposit.

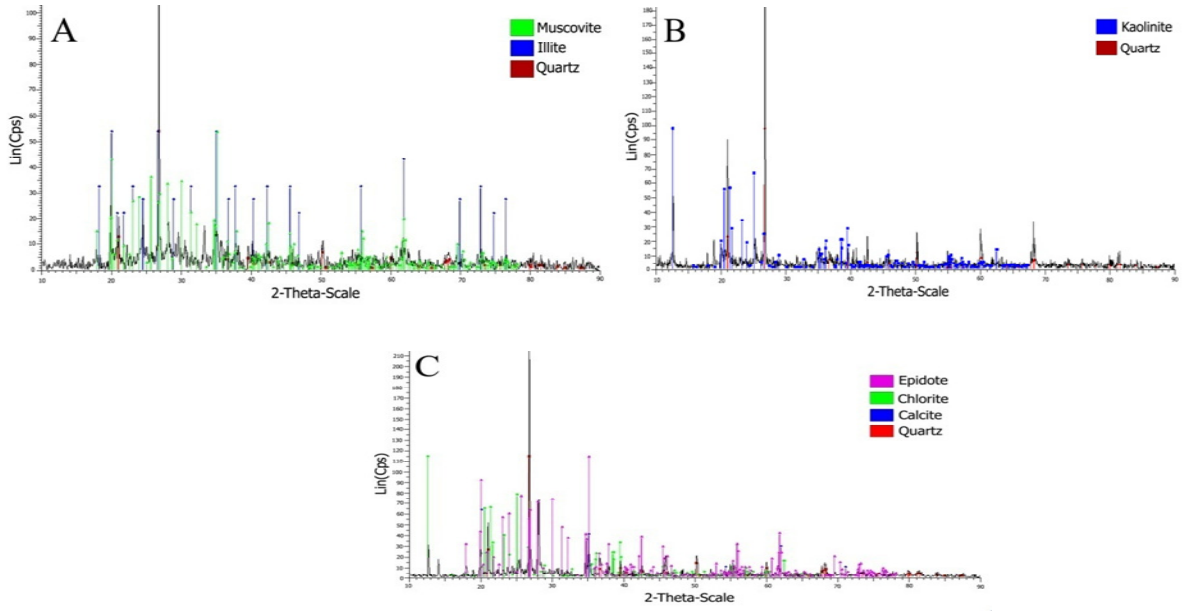

Figure 11. Results of XRD for specific alteration zones (A) Phyllic rock sample; (B) Argillic rock sample; (C) Prophylitic rock sample.

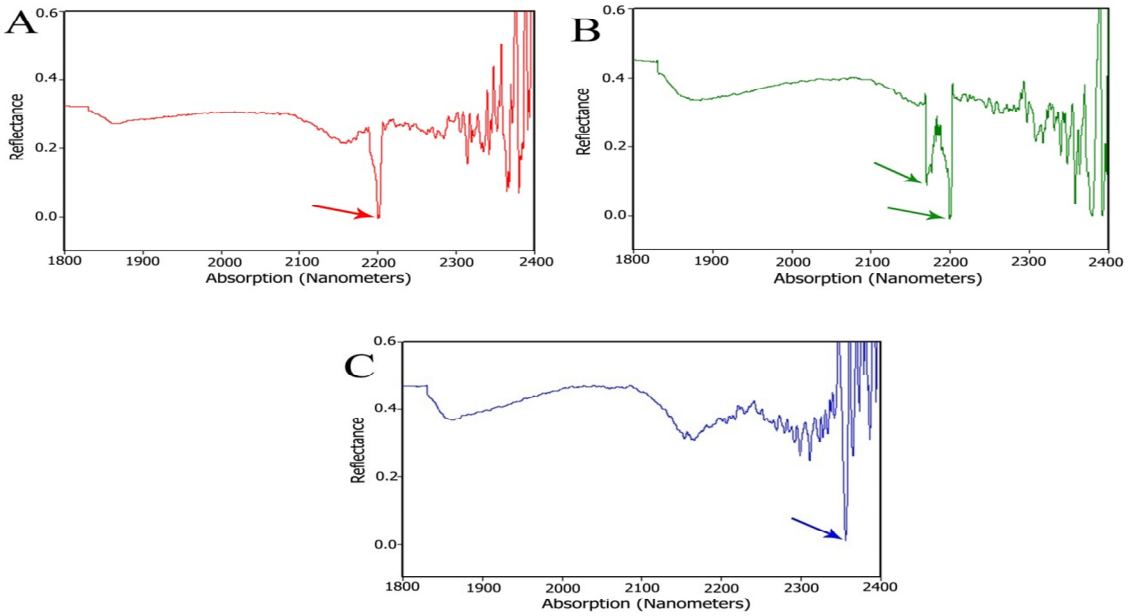

Figure 12. Laboratory reflectance spectra of alteration rock samples, arrows pointed the maximum absorption (A) Phyllic rock sample has maximum absorption in 2200 nm; (B) Argillic rock sample has maximum absorption in 2170 and 2200 nm; (C) Propylitic rock sample has maximum absorption in 2350 nm.

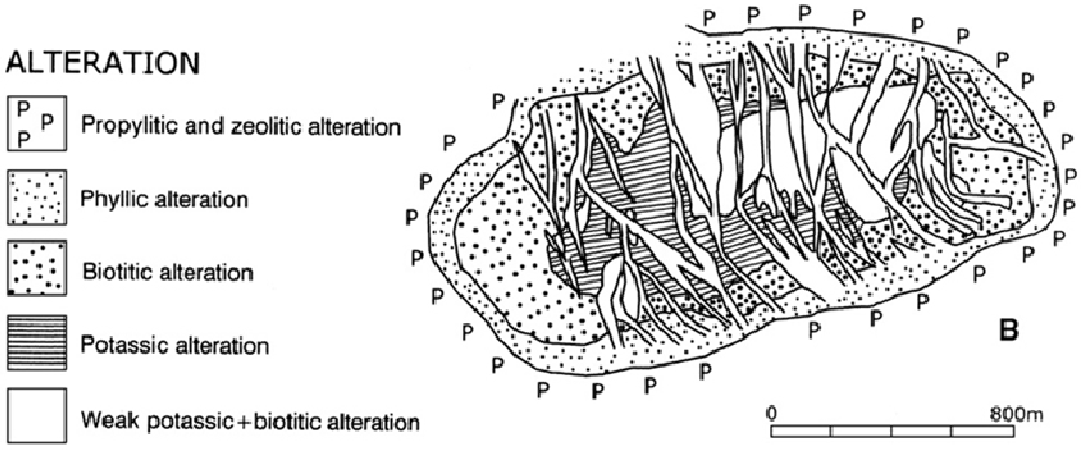

Figure 13. Alteration map of Sarcheshmeh porphyry copper mine. Phyllic and propylitic zones were identified by processed images.

CONCLUSIONS

This study presents specific example of the advantages of spectral mapping techniques such as spectral angle mapping (SAM), linear spectral unmixing (LSU), matched filtering (MF), and mixture tuned matched filtering (MTMF) on SWIR of ASTER data. The spectral properties of reference minerals from the ASTER spectral library version 2.0 were used for the identification of high potential alteration zones associated with hydrothermal porphyry copper mineralization. Results exhibited that these image processing techniques are reliable and robust, fast and can be extrapolated to similar or virgin regions as initial steps of mineral exploration for the identification of high potential copper mineralized lithological units. The techniques were applied on two well-known copper mining districts in SE Iran and their reliability was confirmed with the field and experimental

results.

ACKNOWLEDGEMENTS

This study is conducted as part of Fundamental Research Grant Scheme, Ministry of Higher Education Malaysia. We are grateful to the University Technology Malaysia for providing the facilities, finance and laboratory equipments for this investigation. We also thank reviewers for their comments, which were especially helpful for clarifying certain points in the manuscript.

REFERENCES

Abrams M (2000). The Advanced Spaceborne Thermal Emission and Reflection Radiometer (ASTER): Data products for the high spatial resolution imager on NASA's Terra platform. Intell. J. Rem. Sens., 21: 847-859.

Abrams M, Hook SJ (1995). Simulated ASTER data for geologic studies. IEEE Trans. Geosci. Remote. Sens., 33(3).

Aftabi A, Atapour H (1997). Geochemical and petrological characteristics of shoshonitic and potassic calcalkaline magmatism at Sarcheshmeh and Dehsiahan porphyry copper deposits, Kerman, Iran. Res. Bull. Isfahan Univ., 9: 127–156 (in Persian).

Alavi M (1980). Tectonostratigraphic evolution of the Zagros-sides of Iran. Geology, 8: 144-149.

Amidi SM (1984). Geological map of the Saveh quadrangle: Tehran, Geological Survey of Iran (scale 1:250,000).

Amiraie A (1991). The study of mineralization and hydrothermal alteration at Meiduk porphyry copper deposit. M.Sc. Thesis. Shiraz Univ., p. 125 (in Persian).

Baldridge AM, Hook SJ, Grove CI, Rivera G (2009).The ASTER spectral library version 2.0. Rem. Sens. Environ., 113: 711-715.

Ben-Dor E, Kruse FA, Lefkoff AB, Banin A (1994). Comparison of three calibration techniques for utilization of GER 63-channel aircraft scanner data of Makhtesh Ramon, Nega, Israel. Photo. Eng. Rem. Sens., 60(11): 1339-1354.

Berberian F, Muir ID, Pankhurst RJ, Berberian M (1982). Late Cretaceous and early Miocene Andean type plutonic activity in northern Makran and central Iran. J. Geol. Soc. London, 139: 605-614.

Boardman JW (1992). Sedimentary facies analysis using imaging spectrometry: A geophysical inverse problem. Unpublished Ph.D. Thesis, Univ. Colorado.

Boardman JW (1998). Leveraging the high dimensionality of AVIRIS data for improved sub-pixel target unmixing and rejection of false positives: Mixture tuned matched filtering. In: Summaries of the Seventh Annual JPL Airborne Geoscience Workshop, Pasadena, CA, p. 55.

Boardman JW, Kruse FA, Green RO (1995). Mapping target signatures via partial unmixing of AVIRIS data summaries. Proceedings of the Fifth JPL Airborne Earth Science Workshop, 23–26 January, Pasadena, California, JPL Publ., 95–1. 1: 23–26.

Boomeri M, KazuoN, David RL (2009). The Miduk porphyry Cu deposit, Kerman, Iran: A geochemical analysis of the potassic zone including halogen element systematics related to Cu mineralization processes. J. Geochem. Explor., 103: 17–29.

Castro L AI (2004). An assessment on the potential of mapping hydrothermal alteration from ASTER short wavelength infrared image data based on image simulation experiment. Unpublished M.Sc. thesis. International Institute for Geo-information Science and Earth Observation, Enscheda, The Netherlands.

Di Tommaso I, Rubinstein N (2007). Hydrothermal alteration mapping using ASTER data in the Infiernillo porphyry deposit. Argentina Ore. Geo. Rev., 32: 275-290.

Dimitrijevic MD (1973). Geology of Kerman region. Geological Survey of Iran Rep., 52: 334.

Ducart DF, Crosta AP, Filio CRS (2006). Alteration mineralogy at the Cerro La Mina epithermal prospect, Patagonia, Argentina: Field mapping, short-wave infrared spectroscopy, and ASTER images. Eco. Geo., 101: 981-996.

Farhoudi G (1978). A comparison of Zagros geology to island arcs. J. Geo., 86: 323-334.

Forster H, Fesefeldt K, Ku¨rsten M (1972). Magmatic and orogenic evolution of the central Iranian volcanic belt. 24th Int. Geol. Congr. Sect.,, 2: 198-210.

Hajian H (1977).Geological map of the Tafresh area: Tehran, Geological Survey of Iran, scale 1:100,000.

Hassanzadeh J (1993). Metallogenic and tectonomagmatic events in the SE sector of the Cenozoic active continental margin of central Iran (Shahr-e-Babak area, Keman Province) [Ph.D. thesis]: Los Angeles, University of California, Los Angeles, p. 204.

Hezarkhani A (2006). Hydrothermal evolution of the Sar-Cheshmeh porphyry Cu–Mo deposit, Iran: Evidence from fluid inclusions. J. Asian Ear. Sci., 28: 409-422.

Huber H (1969). Geological map of Iran sheet no. 5, southcentral Iran: Tehran, National Iranian Oil Company, scale, 1:1,000,000.

Hunt GR, Ashley P (1979). Spectra of altered rocks in the visible and near infrared. Eco. Geo., 74: 1613-1629.

Iwasaki A, Tonooka H (2005). Validation of a crosstalk correction algorithm for ASTER/SWIR. IEEE Trans. Geo. Rem. Sens., 43(12): 2747-2751.

Jacobsen JBJ (1975). Copper deposits in time and space. Miner. Sci. Eng., 7(4): 337–371.

Kruse FA, Boardman JW, Lefkoff AB, Heidebrecht KB, Shapiro AT, Barloon PJ, Goetz AFH (1993). The Spectral Image Processing System (SIPS) – Interactive Visualization and Analysis of Imaging Spectrometer Data. Rem. Sens. Environ., 44: 145-163.

Lowell JD, Guilbert JM (1970). Lateral and vertical alteration-mineralization zoning in porphyry ore deposits: Econ. Geol. Bull. Soc. Econ. Geol., 65(4): 373-408.

Mars JC, Rowan LC (2006). Regional mapping of phyllic- and argillic-altered rocks in the Zagros magmatic arc, Iran, using Advanced Spaceborne Thermal Emission and Reflection Radiometer (ASTER) data and logical operator algorithms. Geosphere, 2(3): 161-186.

Ranjbar H, Honarmand M, Moezifar Z (2004). Application of the Crosta technique for porphyry copper alteration mapping, using ETM+ data in the southern part of the Iranian volcanic sedimentary belt. J. Asian Earth Sci., 24: 237–243.

Regard V, Bellier O, Thomas JC, Abbassi MR, Mercier J, Shabanian E, Feghhi K, Soleymani S (2004). Accommodation of Arabia-Eurasia convergence in the Zagros-Makran transfer zone, SE Iran: A transition between collision and subduction through a young deforming system. Tectonics, 23(4): 24.

Rowan LC, Robert GS, John C (2006). Distribution of hydrothermally altered rocks in the Reko Diq, Pakistan mineralized area based on spectral analysis of ASTER data. Rem. Sens. Environ., 104: 74-87.

Shafiei B (2010). Lead isotope signatures of the igneous rocks and porphyry copper deposits from the Kerman Cenozoic magmatic arc (SE Iran), and their magmatic-metallogenetic implications. Ore Geo. Rev., (Article in press), doi:10.1016/j.oregeorev.2010.05.004.

Shafiei B, Haschke M, Shahabpour J (2009). Recycling of orogenic arc crust triggers porphyry Cu mineralization in Kerman Cenozoic arc rocks, southeastern Iran. Miner. Depos., 44: 265-283.

Shahabpour J (2005). Tectonic evolution of the orogenic belt in the region located between Kerman and Neyriz. J. Asian Earth Sci., 24: 405-417.

Shahabpour J (2007). Island-arc affinity of the Central Iranian Volcanic Belt. J. Asian Earth Sci., 30: 652-665.

Stocklin J (1974). Possible ancient continental margins in Iran. In: Burk,C.A., Drake, C.L. (Eds.), The Geology of Continental Margins, Springer, Berlin, pp. 873-887.

Tangestani MH, Mazhari N, Ager B, Moore F (2008). Evaluating advance spaceborne thermal emission and reflection radiometer (ASTER) data for alteration zone enhancement in a semi-arid area,

northern shahr-e-Babak, SE Iran. Int. J. Rem. Sens., 29(10): 2833-2850.
Tangestani MH, Moore F (2002). "Porphyry copper alteration mapping at the Meiduk area, Iran." Int. J. Rem. Sens., 23(22): 4815-4825.
Thome K, Palluconi F, Takashima T, Masuda K (1998). Atmospheric Correction of ASTER. IEEE Trans. Geo. Rem. Sens., 36(4): 1119-1211.
Waterman GC, Hamilton RL (1975). The Sarcheshmeh porphyry copper deposit. Eco. Geo., 70: 568-576.
Yamaguchi YI, Fujisada H, Kudoh M, Kawakami T, Tsu H, Kahle AB, Pniel M (1999). ASTER instrument characterization and operation scenario. Adv. Space Res., 23(8): 1415-1424.